PLEASE CITE THIS ARTICLE AS DOI: 10.1063/5.0110769

### Focused Surface Acoustic Wave induced nanooscillator based reservoir computing

Md. Fahim F. Chowdhury<sup>1</sup>, Walid Al Misba<sup>1</sup>, Md Mahadi Rajib<sup>1</sup>, Alexander J. Edwards<sup>2</sup>, Dhritiman Bhattacharya<sup>3</sup>, Mathew S. Varghese<sup>2</sup>, Joseph S. Friedman<sup>2</sup>, Jayasimha Atulasimha<sup>1\*</sup>

<sup>1</sup>Department of Mechanical and Nuclear Engineering, Virginia Commonwealth University, Richmond, VA, USA

<sup>1</sup>{chowdhurymf, misbawa, rajibmm, jatulasimha}@vcu.edu

<sup>2</sup>Department of Electrical and Computer Engineering, The University of Texas at Dallas, Richardson, TX, USA

<sup>2</sup>{alexander.edwards, Mathew.Varghese, joseph.friedman}@utdallas.edu

<sup>3</sup>Department of Physics, Georgetown University, Washington, DC, USA

<sup>3</sup>dhritiman.bhattacharya@georgetown.edu

\*Authors to whom correspondence should be addressed: Jayasimha Atulasimha, jatulasimha@vcu.edu

We demonstrate using micromagnetic simulations that a nanomagnet array excited by Surface Acoustic Waves (SAWs) can work as a reservoir. An input nanomagnet is excited with focused SAW and coupled to several nanomagnets, seven of which serve as output nanomagnets. To evaluate memory effect and computing capability, we study the Short-Term Memory (STM) and Parity Check (PC) capacities respectively. The SAW (4 GHz carrier frequency) amplitude is modulated to provide sequence of sine and square waves of 100 MHz frequency. The responses of the selected output nanomagnets are processed by reading the envelope of their magnetization state, which is used to train the output weights using regression method. For classification, a random sequence of 100 square and sine wave samples are used, of which 80% are used for training, and the rest are used for testing. We achieve 100% training and 100% testing accuracy. The average STM and PC are calculated to be ~4.69 bits and ~5.39 bits respectively, which is indicative of the proposed acoustically driven nanomagnet oscillator array being well suited for physical reservoir computing applications. The energy dissipation is ~2.5 times lower than a CMOS-based echo-state network. Furthermore, the reservoir is able to accurately predict Mackey-Glass time series up to several time steps ahead. Finally, the ability to use high frequency SAW makes the nanomagnet reservoir scalable to small dimensions and the ability to modulate the envelope at a lower frequency (100 MHz) adds flexibility to encode different signals beyond the sine/square waves demonstrated here.

**Keywords:** Reservoir computing (RC), recurrent neural network (RNN), neuromorphic computing, surface acoustic wave (SAW), spintronics.

A Recurrent Neural Network (RNN) is a machine learning algorithm, which uses its internal memory to remember previous inputs and hence process time-series data e.g., speech, audio, text, weather, etc. Reservoir Computing (RC) is derived from the RNN theory and is a computational framework where a fixed, non-linear reservoir maps the inputs into higher-dimensional space and the readout is trained with linear regression and classification<sup>1</sup>. A RC network consists of inputs, reservoirs, and outputs as shown in Fig. 1(a). In a RC network, only the output weights are trained with a fast and simple linear regression method, which enables the implementation of efficient

# This is the author's peer reviewed, accepted manuscript. However, the online version of record will be different from this version once it has been copyedited and typeset PLEASE CITE THIS ARTICLE AS DOI: 10.1063/5.0110769

training. Such physical reservoir implementations are suitable for edge devices that need to learn in real-time with limited hardware, computational resources, and energy. An ideal physical reservoir should have short-term memory effect and non-linear dynamics as well as be amenable to manufacturing with minimal circuitry. Various Physical RC (PRC) systems are proposed by researchers such as spintronic PRC<sup>2-12</sup>, electronic PRC<sup>2</sup>, photonic PRC<sup>13-14</sup>, etc. Each of these physical reservoirs has respective advantages and disadvantages.

Spintronic nanomagnetic devices are particularly well suited for physical reservoir computing due to their inherent interactive non-linear dynamics, recurrence characteristics, enduring lifetime, CMOS-compatibility, and low energy consumption<sup>2-3</sup>. Spintronic PRC has been simulated or experimentally implemented using dipole-coupled nanomagnets<sup>15-16</sup>, spin-torque-nano-oscillators (STNOs)<sup>10,17-18</sup>, spin-wave systems<sup>19-21</sup>, and different skyrmion fabrics<sup>4-6,22</sup>. Simple pattern recognition task can be performed with a skyrmion fabric reservoir, which utilizes the recursive response of magnetization dynamics<sup>5</sup>. Complex tasks such as image classification can also be performed by a single magnetic skyrmion memristor (MSM) with current pulse stimulation<sup>4,6</sup>. Several studies have proposed domain wall (DW) based neurons and synapses for integrated hybrid CMOS and spintronic computing<sup>7-9</sup>. Apart from skyrmion textures and DWs, vortex-type spin-torque-oscillator<sup>10</sup>, magnetic-dipole interactions<sup>15</sup> can be used as a resource for nonlinear dynamics of a spintronic reservoir. Higher computational capabilities can be achieved using forced synchronization<sup>10</sup>, by increasing the number of STNOs, or at the boundary between synchronized and disordered states<sup>23</sup>.

Recently, strain-mediated nanomagnet devices  $^{28-29}$  were demonstrated for memory applications through resonant surface acoustic wave (r-SAW) assisted spin-transfer-torque  $^{24-25}$ . Unlike memory application, reservoir computing does not require the nanomagnets to switch to an orthogonal state or undergo a complete reversal. Hence, the energy barrier ( $E_b = K_u V \sim 1eV$ ) constraint, associated with volume (V), and perpendicular anisotropy constant ( $K_u$ ) is not critical to its working. The SAW induced stress at a suitable frequency can induce ferromagnetic resonance, which leads to large amplitude precession while being energy efficient. These advantages motivated us to propose SAW induced magnetization dynamics as an input to nanomagnetic reservoirs. SAWs are generated by an inter-digitated-transducer (IDT) patterned on a piezoelectric substrate, which produces Raleigh (transverse) waves. Piezoelectric materials such as Lithium Niobate ( $LiNbO_3$ ), can be used to generate such SAW waves that induce magnetization dynamics in magnetostrictive nanomagnets.

In this work, we demonstrate via micromagnetic simulation that a nanomagnet array, shown in Fig. 1, excited by SAW can be used as a reservoir to classify sine and square waves with high accuracy. We also evaluate two figures of merit tasks of RC named short-term memory (STM) capacity and parity check (PC) capacity. The STM and PC capacity tasks characterize the memory effect (influence of past states) and computing capability (non-linearity) of the system, respectively<sup>26</sup>. The amplitude of the SAW applied to the input nanomagnet is modulated in such a

PLEASE CITE THIS ARTICLE AS DOI: 10.1063/5.0110769

way that its envelope forms random sequence of sine and square waves of 100 MHz frequency. The non-linear responses of the output nanomagnets due to such an input are processed by reading the reservoir state in certain intervals and then trained to classify sine and square waves and calculate STM and PC capacity.

Piezoelectric substrate

Output

Output

Output

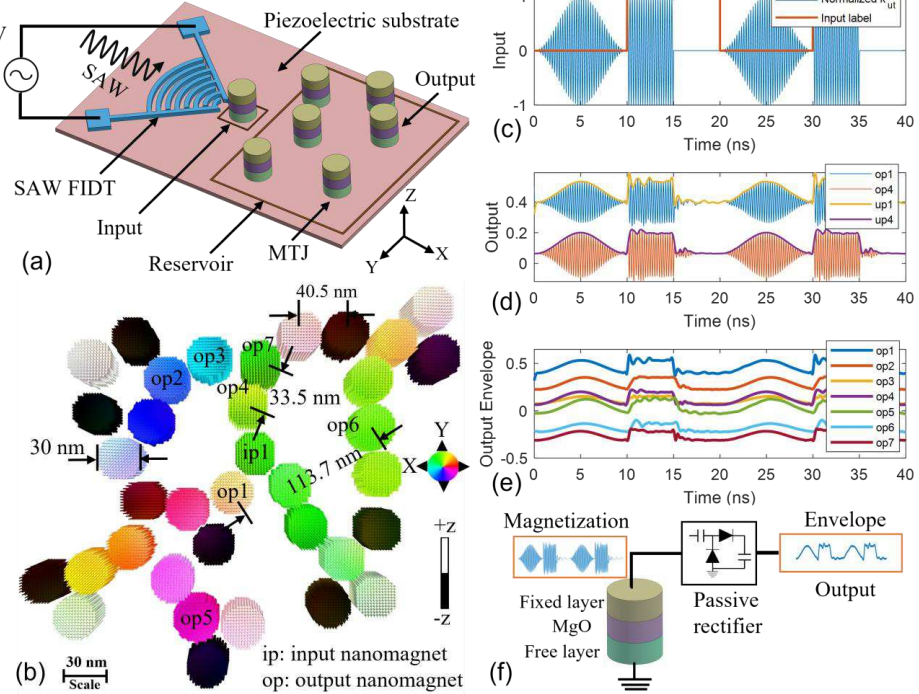


Fig. 1: (a) Conceptual schematic showing application of SAW with Focused Inter-Digitated Transducer (FIDT) on the input nanomagnet as well as reservoir and output nanomagnets. (b) A micro-magnetic snapshot of the input, the reservoir, and the output nanomagnets. The SAW is applied to the input nanomagnet (ip1) and the magnetizations of the output nanomagnets (op1 to op7) are read. (c) Normalized stress anisotropy and labeling of sine and square waves as 1 and 0. (d) Magnetization of output nanomagnets 1 (op1) and 4 (op4) in response to SAW and their corresponding envelopes (up1 and up4). (e) The envelopes of the responses vs. time (ns) of several output nanomagnets. (f) Electrical readout of the magnetization of the output nanomagnet softlayer with an MTJ.

We obtain the free layer magnetization dynamics of the reservoir through micromagnetic simulation with MuMax3<sup>27</sup>. The magnetization direction of the reference ferromagnetic layer of an MTJ is fixed and the free layer magnetization is governed by the Landau-Lifshitz-Gilbert (LLG) (see supplementary) equation as follows:

### AIP Publishing

This is the author's peer reviewed, accepted manuscript. However, the online version of record will be different from this version once it has been copyedited and typeset PLEASE CITE THIS ARTICLE AS DOI: 10.1063/5.0110769

Here,  $\vec{m}$  is the normalized magnetization defined as  $\frac{\vec{M}}{M_S}$ ,  $\vec{M}$  is the magnetization,  $M_S$  is the saturation magnetization,  $\alpha$  is the Gilbert damping coefficient,  $\gamma$  is the gyromagnetic ratio.

We assume a uniform stress induced by the SAW within the magnetic domain in the  $\vec{u}$  direction and the stress creates a purely uniaxial anisotropy. We note that the estimated stress amplitude is conservative due to this assumption, but the qualitative magnetization dynamics remain the same. Since the focused SAW is locally applied to the region of the input magnet only, the induced stress in the piezoelectric substrate in the reservoir or output region is comparatively negligible. So, the stress anisotropy field,  $\vec{H}_{stress\,anis}=0$  and the effective field on the nanomagnets of the reservoir or output nanomagnets is comprised of  $\vec{H}_{demag}$  and  $\vec{H}_{exchange}$ .  $\vec{H}_{demag}$  is calculated by MuMax<sup>27</sup> at every point in each nanomagnet due to shape anisotropy of the nanomagnet itself and due to dipole coupling from other nanomagnets.

The application of focused SAW on the piezoelectric substrate induces stress anisotropy and causes magnetization precession in the input nanomagnet, ip1. Closely placed nanomagnets are dipole-coupled and start precession due to the coupling with the input nanomagnet. These nanomagnets further couple with other nanomagnets forming a reservoir of dipole-coupled nanomagnets. The magnetic-dipole interactions in the nanomagnets create recurrent loops which can induce memory functionality to the array. The coupled nanomagnets act like synapse weights in a neural network and the weights of the reservoir synapses are fixed which depends on the intermagnetic relative geometrical coordinates in the array. The array of nanomagnets which forms the reservoir are patterned in an irregular layout to add asymmetry, to further enrich the reservoir.

Fig. 1(a,b) shows the schematic of the proposed reservoir with the application of focused SAW. The input nanomagnet is indicated by ip1 and output nanomagnets are denoted by op1 to op7. We assume a 4 GHz SAW is applied to the input nanomagnet using a focused interdigitated transducer (FIDT), which is patterned on top of a piezoelectric. The SAW input and its propagation in the piezoelectric substrate are not modeled in MuMax3 simulation, and the SAW input is given only through the uniaxial stress anisotropy constant,  $k_{ut}$  term in equation 3. The simulation dimension is  $256 \times 256 \times 16$  cells which covers all input, reservoir, and output nanomagnets, and each cell size is  $2nm \times 2nm \times 2.1875nm$ , which is much lower than the ferromagnetic exchange length,  $\sqrt{2A_{ex}/\mu_0 M_s^2} = 6.32nm$ . The material and simulation parameters<sup>39-43</sup> are summarized in Table I.

PLEASE CITE THIS ARTICLE AS DOI: 10.1063/5.0110769

Table I. Simulation and material parameters for the physical reservoir for the soft ferromagnetic CoFe<sup>39-43</sup> layer.

| Parameter                          | Value                          |
|------------------------------------|--------------------------------|
| Gilbert damping constant, $\alpha$ | 0.05                           |
| Saturation magnetization, $M_s$    | $0.72 \times 10^6 \text{ A/m}$ |
| Exchange stiffness, $A_{ex}$       | 13 x 10 <sup>-12</sup> J/m     |
| Free layer thickness, t            | 35 nm                          |
| Nanomagnet diameter, D             | 30 nm                          |
| Magnetostriction, $\lambda_s$      | 250 ppm                        |

Two fundamental properties required for reservoir computing are nonlinearity and memory<sup>38</sup>. Due to the nonlinearity and complex dynamics of the reservoir, the network response should be consistent/similar for similar inputs and distinguishable for different inputs<sup>30</sup>. For RC, we utilize the magnetization dynamics of the input and output nano-oscillators, which are governed by the LLG equation described earlier. Further, the input information is encoded in the envelope of a focused SAW of 4 GHz consisting of a random sequence of sine and square waves. The details of the RC method are presented in the supplementary.

We evaluate the quantitative performance of the reservoir with STM task and PC task<sup>30</sup>. STM task characterizes the memory effect of the system by generating delayed inputs and testing if the internal dynamics of the reservoir is trained to adjust to this delay. Input data,  $i_s(n)$  is delayed by arbitrary unit, d and STM task is to identify the delayed input,  $y_{STM}^{n,d}$ :

$$y_{STM}^{n,d} = i_s(n-d) \tag{2}$$

here,  $i_s(n)$  represents the  $n^{th}$  sine/square signal and d is the introduced delay. The duration of each of the sine/square signal is 10 ns, thus delay, d = 1 corresponds to 10 ns and so on.

Since the STM task is not sufficient to prove reservoir property, the PC task is also evaluated as a benchmark task. The PC task characterizes the non-linearity of the system, which is indicative of the computing capability of the system and simplifies the training of the reservoir. A modulo (2) operation, which introduces non-linearity, is performed on the summation of input signal  $i_s(n)$  up to delay, d to obtain PC task output,  $y_{PC}^{n,d}$ :

$$y_{PC}^{n,d} = [i_s(n-d) + i_s(n-d+1) + \dots + i_s(n)] \mod(2); \ d \neq 0$$
 (3)

In Eq 2-3,  $y_{STM/PC}^{n,d}$  represents the training and testing data for STM and PC tasks for various delays. Once the learned weights are obtained, the correlation coefficient between testing data, and output

PLEASE CITE THIS ARTICLE AS DOI: 10.1063/5.0110769

### AIP

data  $y_{out}$  are calculated. The total capacities for STM ( $C_{STM}$ ) and PC ( $C_{PC}$ ) tasks are calculated by integrating (summing in the discrete case) the correlation coefficients for delay up to  $d_{max}$ .

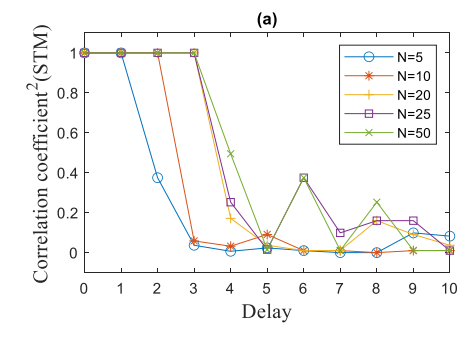
$$r_{STM/PC}(d) = \sqrt{\frac{covariance[y_{STM/PC}^{n,d}]}{variance[y_{STM/PC}]variance[y_{out}]}}$$
(4)

$$C_{STM/PC} = \sum_{d=1}^{d_{max}} \left[ r_{STM/PC}(d) \right]^2$$
 (5)

The nanomagnets are realized by magnetic tunnel junctions (MTJs), made of two CoFe layers (free and reference) separated by a tunnel barrier (MgO). The free layer magnetization responses of the outputs are read and preprocessed to obtain envelopes by spline interpolation<sup>31</sup> over local maxima separated by at least 3 samples. The envelopes of the output nanomagnets are shown in Fig. 1(e). Each sine or square signal is sampled into N nodes separated by a sampling time  $\tau$ . The node density can be increased by introducing virtual nodes<sup>32-33</sup>. The weights are obtained by the linear regression method.

To quantify the performance of the proposed reservoir, the sine and square wave classification is performed by the reservoir as a first task. Although simple, this classification task requires non-linearity and memory effects of the system to predict or classify these waves with high accuracy. The input is a random sequence of 100 sine and square waves with equal period of 10 ns. The first 80 signals are used to train, and the next 20 signals are used to test the reservoir for signal classification, STM task, and PC tasks. The reservoir is able to achieve 100 % training and 100 % testing accuracy with any of the output nanomagnets. The training and testing are performed for the different numbers of virtual nodes 5, 10, 20, 25, and 50, where 100 % recognition rate in both training and testing was achieved for all cases.

To further evaluate the performance of the reservoir, we studied two fundamental characteristics: fading memory and non-linearity<sup>38</sup>. To evaluate the memory of the reservoir we have calculated STM capacity and to evaluate the nonlinearity, we have performed the PC task and results are discussed next.



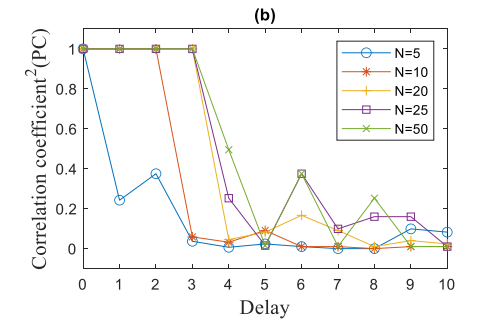


Fig. 2(a) shows the square of the correlation coefficient,  $r_{STM}^2(d)$  between the training data of STM task,  $y_{STM}^{n,d}$  and output data,  $y_{out}$  as a function of delay from d=0 to d=10. Each of the time steps correspond to a 10 ns delay. The STM correlation coefficient<sup>2</sup>,  $r_{STM}^2 = 1$  for all the number of virtual nodes, N in consideration at delay, d=1 and starts to decrease with the increase of the delay. The  $r_{STM}^2(d)$  tends to be higher in general with the increase in the number of the virtual nodes. Similarly, Fig. 2(b) presents the square of the correlation coefficient,  $r_{PC}^2(d)$  between the training data of PC task,  $y_{PC}^{n,d}$  and output data,  $y_{out}$  as a function of delay from d=0 to d=10. Similar trends as STM have been observed for the PC task, for the correlation coefficient, as a function of the number of virtual nodes, and delay.

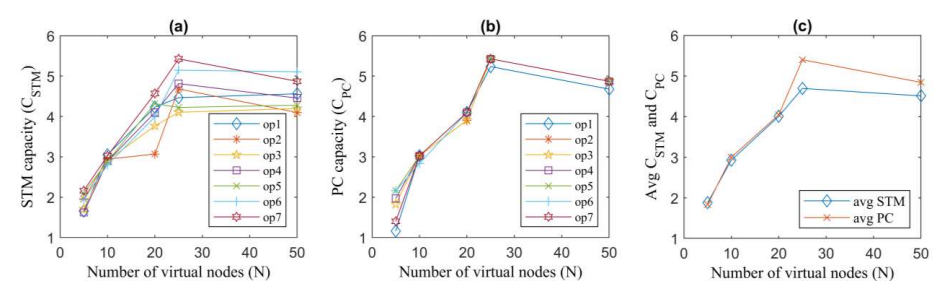


Fig. 3: (a) STM capacity  $(C_{STM})$  and (b) PC capacity  $(C_{PC})$  of the reservoir as a function of the number of virtual nodes (c) Average STM and PC capacity of the reservoir as a function of the number of virtual nodes.

The dependency of STM capacity ( $C_{STM}$ ) on the number of virtual nodes, N in each signal is shown in Fig. 3(a). There is a general tendency of increasing STM capacity with an increasing number of virtual nodes for all the output nanomagnets. Fig. 3(b) shows the PC capacity  $(C_{PC})$  vs. virtual node numbers (N) follows similar characteristics as STM task. The maximum capacity achieved by the reservoir for both STM and PC tasks is 5.43 bits for the case with output nanomagnet op7 and 25 virtual nodes. The obtained STM and PC capacities are comparable or higher than the other spintronic reservoirs 10,23,26,34. The average STM and PC capacity of seven output nanomagnets are shown in Fig. 3(c) in terms of the virtual node numbers. The reservoir has an average STM capacity of ~4.69 and PC capacity of ~5.39 bits. The reservoir can be tuned for optimal performance of the STM and PC capacities through parameter study of the materials (e.g., damping constant ( $\alpha$ ), saturation magnetization ( $M_s$ ), exchange stiffness ( $A_{ex}$ ) etc.), through dipole coupling strength variation (e.g., optimizing the distances between the nanomagnets), and optimizing the size (diameter/thickness) of the nanomagnets.



PLEASE CITE THIS ARTICLE AS DOI: 10.1063/5.0110769

To separate the role played by the nonlinear nanomagnet reservoir in achieving the high STM and PC over that due to pre-processing (carrier amplitude modulation) and post-processing (filtering the carrier) we perform the following study. The pre-processed input is fed into a single-layer perceptron (SLP) network and its output post-processed before classifying and this is compared to the case of the reservoir with pre and post-processing. The result shows a correlation  $(r^2)$  of 1 for both STM and PC tasks, at delay 1 but very low or almost no correlation  $(r^2)$  for delay 2 and higher compared to the case with filters and reservoir as shown in Fig. 4. The calculated STM and PC capacities of the SLP are  $\sim$ 1.44 bits and  $\sim$ 1.43 bits, respectively while STM and PC capacities of the reservoir are  $\sim$ 3.52 bits and  $\sim$ 3.46 bits, which indicates the effectiveness of the reservoir over merely pre and post-processing.

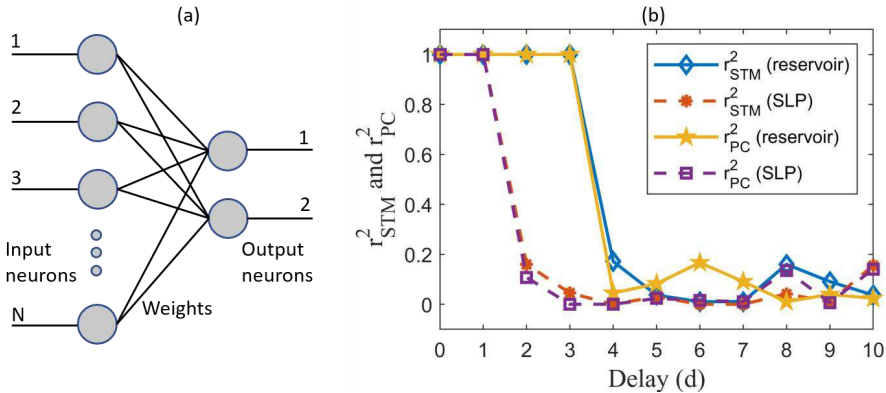


Fig. 4: (a) Architecture of single layer perceptron (SLP) which is used to measure the influence of pre and post-processing on the performance of reservoir (b) Calculated coefficient,  $r_{STM/PC}^2(d)$  for STM and PC tasks with various delay, d for two different cases: with reservoir (solid lines) and without reservoir (only SLP and dashed lines). The number of virtual nodes for both cases are, N=20. The lines are drawn to guide the eye.

To further demonstrate the viability of the reservoir we perform long-term prediction task with Mackey-Glass time series data. This chaotic system has been widely used as a benchmark for forecasting task test due to the difficulty of prediction regardless of the deterministic form of the system  $^{44-46}$ . In Fig. 5 we demonstrate the ability of the reservoir to predict the Mackey-Glass time series for various delays. For each case, 500 data points are used for training and 500 are used for testing and we calculate the mean square error (MSE) to quantify the prediction. The reservoir reproduces the Mackey-Glass input points with MSE of 4.5032  $\times$  10 $^{-7}$  at delay 0, 6.0383  $\times$  10 $^{-4}$  at delay 5, 7.3  $\times$  10 $^{-3}$  at delay 15, and 1.05  $\times$  10 $^{-2}$  delay 30.

# This is the author's peer reviewed, accepted manuscript. However, the online version of record will be different from this version once it has been copyedited and typeset PLEASE CITE THIS ARTICLE AS DOI: 10.1063/5.0110769

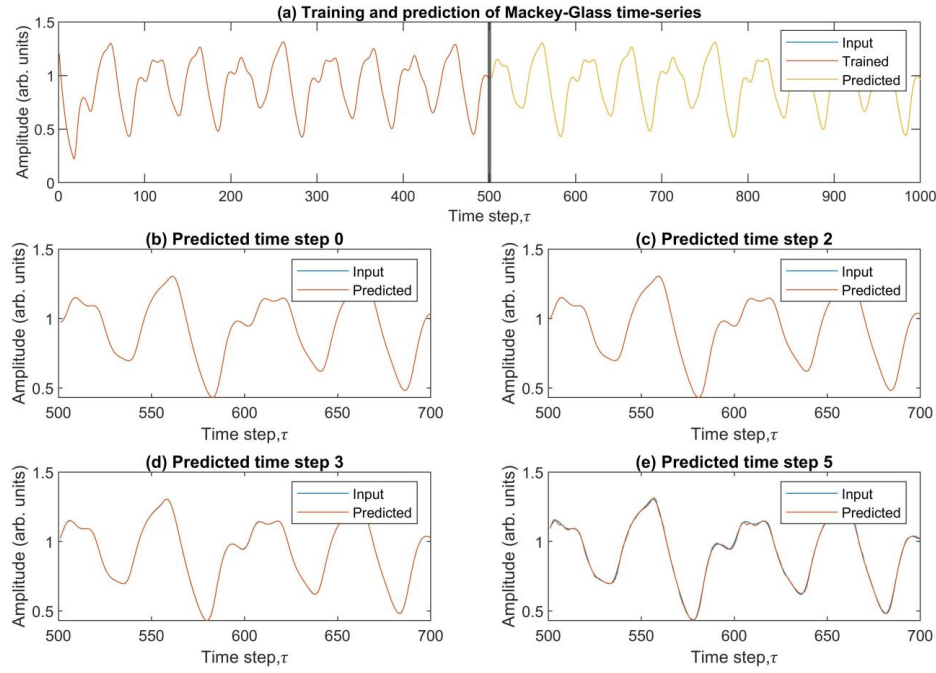


Fig. 5: Forecasting of Mackey-Glass time-series. (a) Training and prediction results obtained from the nanomagnet-based reservoir. Prediction results at (b) Predicted time step=0, (c) Predicted time step=2, (d) Predicted time step=3, (e) Predicted time step=5.

The total energy dissipation in the proposed reservoir system solely depends on the SAW excitation<sup>35-37</sup> as there is no other input mechanism needed. To estimate the energy consumption of the nanomagnets we also assume total generation of SAW induced strain from the piezoelectric substrate to the nanomagnets. The energy dissipated by the focused SAW IDT per input time period is  $\left(\frac{P}{W}\right)Wt_{saw} = 0.87 \text{ pJ}$ , and reservoir output including the trained output layer will consume 84.3 pJ. A CMOS-based echo-state-network (ESN) is simulated to obtain the similar performance of nanomagnet RC and to achieve similar parity check capacity the CMOS ESN needs 11 neurons, which corresponds to 195.7 pJ of energy. So, the total energy dissipation per input is ~85 pJ which is nearly two and a half times lower and energy efficient compared to an equivalent CMOS ESN (see supplementary). Although CMOS ESN is able to achieve comparable accuracies for PC task, the STM task accuracies are still significantly low compared to our spintronic reservoir, which exhibits high capacities for both STM and PC tasks. The energy dissipation can be further decreased by applying higher frequency (> 4GHz) focused SAW, reducing the period of sine/square wave, and carefully selecting or optimizing material parameters. Furthermore, this NMRC scheme requires readout of only a single MTJ and enables the implementation of less external circuitry with more energy saving.

PLEASE CITE THIS ARTICLE AS DOI: 10.1063/5.0110769

In summary, we have introduced a spintronic physical reservoir where a focused SAW is applied to the input. The reservoir is able to identify sine and square waves with 100 % accuracy. In addition, we have demonstrated the expressivity of the reservoir by evaluating two figures of merit for RC and perform the prediction task of a time series data with delay. We have achieved average capacities of ~4.69 and ~5.39 for STM and PC, respectively and reproduce the Mackey-Glass time series data with high accuracy which are indicative of a viable physical reservoir. The reservoir is extremely energy efficient and potentially needs ~2.5 times less energy than a CMOS-based ESN. Finally, the ability to use high-frequency SAW makes the device scalable to small dimensions, while the ability to modulate the envelope at a lower frequency (100 MHz) adds flexibility to encode different signals beyond the work in this paper. This could be key to applications such as speech recognition, anomaly detection, etc. using in-situ learning in edge devices. ACKNOWLEDGEMENT M.F.F.C., W.A.M., M.M.R., and J.A. are supported in part by the National Science Foundation

grant CCF-1815033 and Commonwealth Cyber Initiative (CCI).

### **AUTHOR DECLARATIONS**

The authors have no conflicts to disclose

### SUPPLEMENTARY MATERIAL

See supplementary material for details of the reservoir computing method, energy dissipation of SAW, and energy dissipation of CMOS-based echo-state network.

### DATA AVAILABILITY

The data that support the findings of this study are available from the corresponding author upon reasonable request.

### References

- <sup>1</sup>M. Lukoševicius and H. Jaeger, Computer Science Review 3, 127–149 (2009).
- <sup>2</sup>G. Tanaka, T. Yamane, J. B. Héroux, R. Nakane, N. Kanazawa, S. Takeda, H. Numata, D. Nakano, and A. Hirose, Neural Networks 115, 100-123 (2019).
- <sup>3</sup>J. Torrejon, M. Riou, F. A. Araujo, S. Tsunegi, G. Khalsa, D. Querlioz, P. Bortolotti, V. Cros, K. Yakushiji, A. Fukushima, et al., Nature 547, 428-431 (2017).
- <sup>4</sup>G. Bourianoff, D. Pinna, M. Sitte, and K. Everschor-Sitte, Aip Advances 8, 055602 (2018).
- <sup>5</sup>D. Pinna, G. Bourianoff, and K. Everschor-Sitte, Physical Review Applied 14, 054020 (2020).
- <sup>6</sup>W. Jiang, L. Chen, K. Zhou, L. Li, Q. Fu, Y. Du, and R. Liu, Applied Physics Letters 115, 192403 (2019).

PLEASE CITE THIS ARTICLE AS DOI: 10.1063/5.0110769

This is the author's peer reviewed, accepted manuscript. However, the online version of record will be different from this version once it has been copyedited and typeset.

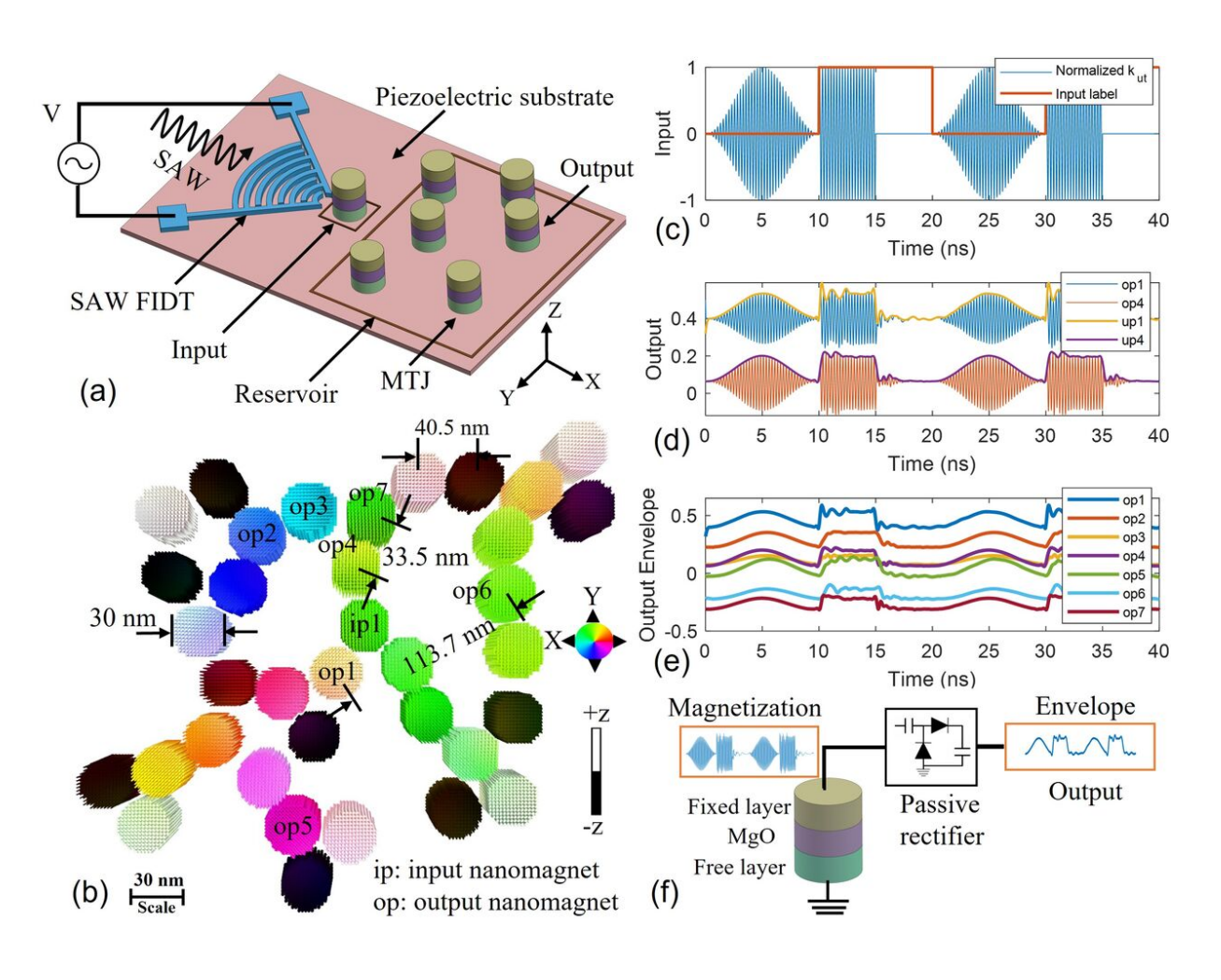
- <sup>7</sup>K. Yue, Y. Liu, R. K. Lake, and A. C. Parker, Science advances 5, eaau8170 (2019).
- <sup>8</sup>S. A. Siddiqui, S. Dutta, A. Tang, L. Liu, C. A. Ross, and M. A. Baldo, Nano letters 20, 1033–1040 (2019).
- <sup>9</sup>R. V. Ababei, M. O. Ellis, I. T. Vidamour, D. S. Devadasan, D. A. Allwood, E. Vasilaki, and T. J. Hayward, Scientific Reports 11, 1–13 (2021).
- <sup>10</sup>S. Tsunegi, T. Taniguchi, K. Nakajima, S. Miwa, K. Yakushiji, A. Fukushima, S. Yuasa, and H. Kubota, Applied Physics Letters 114, 164101 (2019).
- <sup>11</sup>A. J. Edwards, D. Bhattacharya, P. Zhou, N. R. McDonald, L. Loomis, C. D. Thiem, J. Atulasimha, and J. S. Friedman, arXiv preprint arXiv:2103.09353 (2021).
- <sup>12</sup>P. Zhou, N. R. McDonald, A. J. Edwards, L. Loomis, C. D. Thiem, and J. S. Friedman, arXiv preprint arXiv:2003.10948 (2020).
- <sup>13</sup>P. R. Prucnal, B. J. Shastri, T. F. de Lima, M. A. Nahmias, and A. N. Tait, Advances in Optics and Photonics 8, 228–299 (2016).
- <sup>14</sup>T. F. De Lima, B. J. Shastri, A. N. Tait, M. A. Nahmias, and P. R. Prucnal, Nanophotonics 6, 577–599 (2017).
- <sup>15</sup>H. Nomura, H. Kubota, and Y. Suzuki, Reservoir Computing (Springer) pp. 361–374 (2021).
- <sup>16</sup>H. Nomura, K. Tsujimoto, M. Goto, N. Samura, R. Nakatani, and Y. Suzuki, Japanese Journal of Applied Physics 59, SEEG02 (2019).
- <sup>17</sup>D. Markovic, N. Leroux, M. Riou, F. Abreu Araujo, J. Torrejon, D. Quer-´lioz, A. Fukushima, S. Yuasa, J. Trastoy, P. Bortolotti, *et al.*, Applied Physics Letters 114, 012409 (2019).
- <sup>18</sup>M. Riou, J. Torrejon, B. Garitaine, F. A. Araujo, P. Bortolotti, V. Cros, S. Tsunegi, K. Yakushiji, A. Fukushima, H. Kubota, et al., Physical review applied 12, 024049 (2019).
- <sup>19</sup>R. Nakane, G. Tanaka, and A. Hirose, IEEE access 6, 4462–4469 (2018).
- <sup>20</sup>K. Hon, Y. Kuwabiraki, M. Goto, R. Nakatani, Y. Suzuki, and H. Nomura, Applied Physics Express 14, 033001 (2021).
- <sup>21</sup>S. Watt, M. Kostylev, and A. B. Ustinov, Journal of Applied Physics 129, 044902 (2021).
- <sup>22</sup>C.-Y. You and N.-H. Kim, Current Applied Physics 15, 298-301 (2015).
- <sup>23</sup>T. Kanao, H. Suto, K. Mizushima, H. Goto, T. Tanamoto, and T. Nagasawa, Physical Review Applied 12, 024052 (2019).
- <sup>24</sup>A. Roe, D. Bhattacharya, and J. Atulasimha, Applied Physics Letters 115, 112405 (2019).

PLEASE CITE THIS ARTICLE AS DOI: 10.1063/5.0110769

This is the author's peer reviewed, accepted manuscript. However, the online version of record will be different from this version once it has been copyedited and typeset.

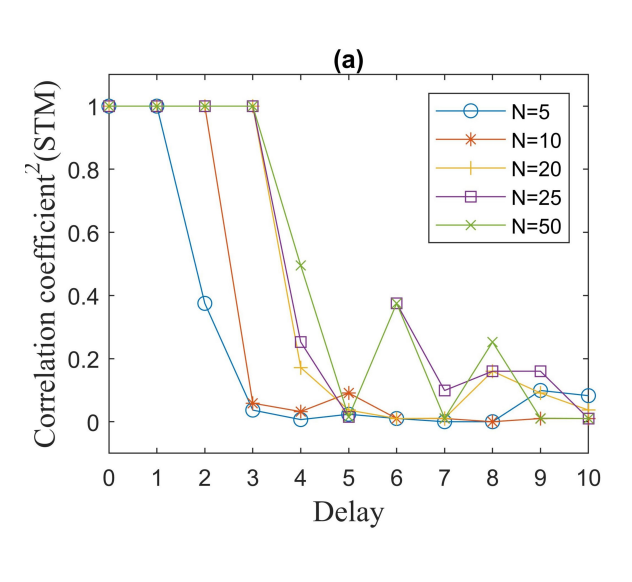
- <sup>25</sup>W. Al Misba, M. M. Rajib, D. Bhattacharya, and J. Atulasimha, Physical Review Applied 14, 014088 (2020).
- <sup>26</sup>T. Furuta, K. Fujii, K. Nakajima, S. Tsunegi, H. Kubota, Y. Suzuki, and S. Miwa, Physical Review Applied 10, 034063 (2018).
- <sup>27</sup>A. Vansteenkiste, J. Leliaert, M. Dvornik, M. Helsen, F. Garcia-Sanchez, and B. Van Waeyenberge, AIP advances 4, 107133 (2014).
- <sup>28</sup>Q. Wang, J. Domann, G. Yu, A. Barra, K. L. Wang, and G. P. Carman, Physical Review Applied 10, 034052 (2018).
- <sup>29</sup>Z. Xiao, (University of California, Los Angeles, 2021).
- <sup>30</sup>N. Bertschinger and T. Natschläger, Neural computation 16, 1413–1436 (2004).
- <sup>31</sup>C. A. Hall and W. W. Meyer, Journal of Approximation Theory 16, 105–122 (1976).
- <sup>32</sup>L. Appeltant, M. C. Soriano, G. Van der Sande, J. Danckaert, S. Massar, J. Dambre, B. Schrauwen, C. R. Mirasso, and I. Fischer, Nature communications 2, 1–6 (2011).
- <sup>33</sup>K. Nakajima, H. Hauser, T. Li, and R. Pfeifer, Soft robotics 5, 339–347 (2018).
- <sup>34</sup>T. Yamaguchi, N. Akashi, K. Nakajima, H. Kubota, S. Tsunegi, and T. Taniguchi, Scientific reports 10, 1–8 (2020).
- <sup>35</sup>M. S. Kharusi and G. W. Farnell, Proceedings of the IEEE 60, 945–956 (1972).
- <sup>36</sup>M. B. Mazalan, A. M. Noor, Y. Wahab, S. Yahud, and W. S. W. K. Zaman, Micromachines 13, 30 (2021).
- <sup>37</sup>S. Datta, (Prentice Hall, 1986).
- <sup>38</sup>W. Maass, T. Natschläger, and H. Markram, Neural computation 14, 2531–2560 (2002).
- <sup>39</sup>H.-G. Piao,H.-C. Choi, J.-H. Shim, D.-H. Kim, and C.-Y. You, Applied Physics Letters 99, 192512 (2011).
- <sup>40</sup>T. Kaisar, M. M. Rajib, H. ElBidweihy, M. Barbic, and J. Atulasimha, Journal of Applied Physics 129, 214505 (2021).
- <sup>41</sup>J. Wang, J. Li, X. Li, X. Bao, and X. Gao, Journal of Magnetism and Magnetic Materials 462, 53–57 (2018).
- <sup>42</sup>J. Huang, W. Song, J. Bain, Y. Yang, L. Shi, T. Schlesinger, T. Chong, and H. Hui, Applied Physics A 113, 221–229 (2013).
- <sup>43</sup>B. Özkale, N. Shamsudhin, T. Bugmann, B. J. Nelson, and S. Pané, Electrochemistry Communications 76, 15–19 (2017).
- <sup>44</sup>H. Jaeger and H. Haas, science 304, 78–80 (2004).
- <sup>45</sup>P. Antonik, M. Haelterman, and S. Massar, Physical Review Applied 7, 054014 (2017).
- <sup>46</sup>J. Moon, W. Ma, J. H. Shin, F. Cai, C. Du, S. H. Lee, and W. D. Lu, Nature Electronics 2, 480–487 (2019).

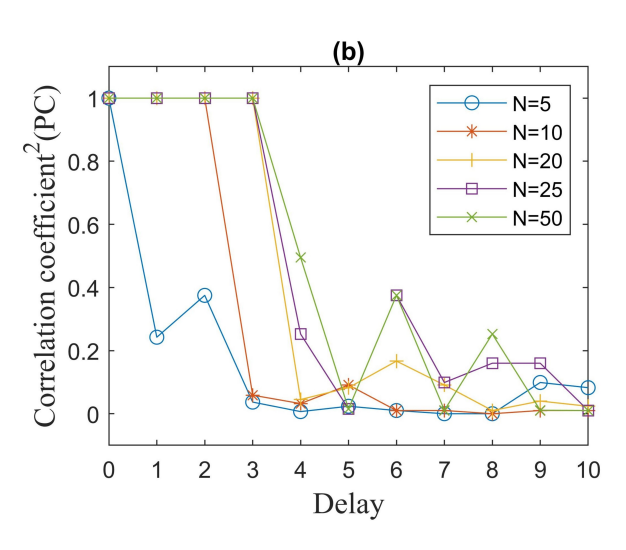
This is the author's peer reviewed, accepted manuscript. However, the online version of record will be different from this version once it has been copyedited and typeset.





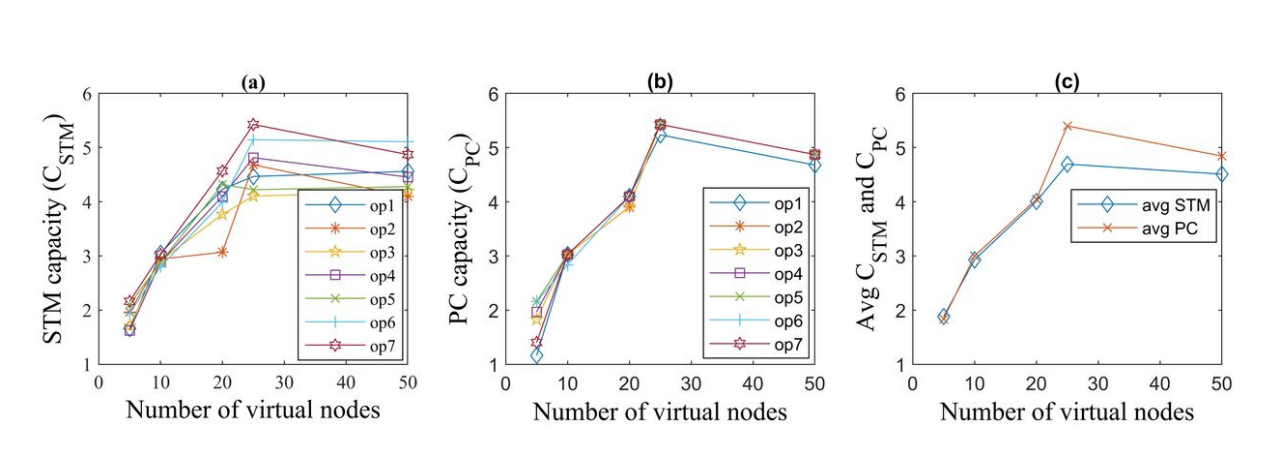
This is the author's peer reviewed, accepted manuscript. However, the online version of record will be different from this version once it has been copyedited and typeset.





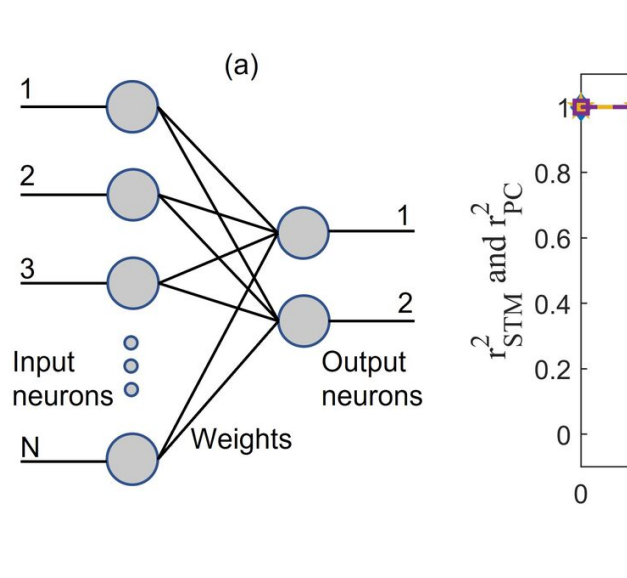


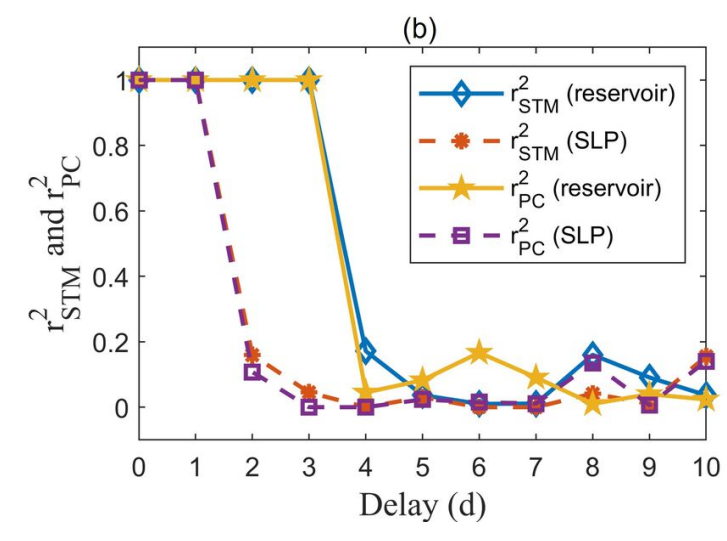
This is the author's peer reviewed, accepted manuscript. However, the online version of record will be different from this version once it has been copyedited and typeset.





This is the author's peer reviewed, accepted manuscript. However, the online version of record will be different from this version once it has been copyedited and typeset.







This is the author's peer reviewed, accepted manuscript. However, the online version of record will be different from this version once it has been copyedited and typeset.

